European Journal of Mechanics A/Solids 66 (2017) 356–369

Contents lists available at ScienceDirect

European Journal of Mechanics A/Solids

journal homepage: www.elsevier.com/locate/ejmsol

Buckling analysis and buckling control of thin films on shape memory polymer substrate

Yuhao He [a, b], Yunxin Li [a], Zishun Liu [a, *], K.M. Liew [b]

[a] Inter. Center for Applied Mechanics, State Key Laboratory for Strength and Vibration of Mechanical Structures, Xi'an Jiaotong University, Xi'an, 710049, China

[b] Department of Civil and Architectural Engineering, City University of Hong Kong, Tat Chee Avenue, Kowloon, Hong Kong

A R T I C L E I N F O

Article history:
Received 11 December 2016
Received in revised form
12 July 2017
Accepted 8 August 2017
Available online 18 August 2017

Keywords:
Buckling
Film/substrate
Theory and simulation
Shape memory polymer

A B S T R A C T

This paper presents a theoretical study and finite element simulation for the buckling of a thin film on the compliant substrate. First, we develop a continuum mechanics approach for large deformation buckling analysis based on minimizing the total energy of the film/substrate structures, and considering the precise curvature of the buckled film and the Poisson's ratio of the substrate. The predicting results using this proposed theory agree quite well with previous experimental results. Then, we make a modification for the model to simplify the expressions for the wavelength and amplitude of the buckled geometry. Furthermore, considering a thin Si film on shape memory polymer (SMP) substrate, we investigate the buckling behavior of the thin film through theoretical analysis and finite element method. Through the investigation, it is found that the evolution rate of the buckling geometry of thin film depends on the temperature of the SMP substrate, and the buckling geometry changes faster at a higher temperature. Finally, a programmed method to control the buckling of thin Si film on the SMP substrate is proposed and is realized with finite element simulation in ABAQUS.

1. Introduction

During the past decades, the thin film/substrate structures have attracted many researchers because of their potential applications in many fields, such as stretchable electronics (Khang and Rogers, 2006; Sun et al., 2006), tunable phase optics (Harrison et al., 2004; Yang and He, 2014), high precision micro- and nano-metrology methods (Stafford et al., 2004, 2006; Wilder et al., 2006; Zhou and Huang, 2014), and pattern formation for micro-/nano-fabrication (Bowden et al., 1998, 1999; Yoo et al., 2002; Chiche et al., 2008; Chen and Crosby, 2014; Alireza and Faramarz, 2015; Park et al., 2015; Wang et al., 2015a; Huang et al., 2016). In these thin film/substrate structures, the fragile and stiff thin films are usually placed on the pre-stretched compliant substrates, and the binding at the interface leads to the bucking of the film.

The buckling phenomenon of thin films on a compliant substrate was first observed by Bowden et al. (1998) when they deposited metal films on a thermally expanded polymer. They also observed that the metal films form wrinkles spontaneously upon cooling. This finding allows them to generate complex ordered wrinkle patterns with wavelengths from sub-micrometer to micrometers (Bowden et al., 1999; Chua et al., 2000; Yoo et al., 2002), and it has been applied in assembling 2D micro/nanomaterials into complex 3D functional architectures by compressive buckling (Dickson, 2015; Xu et al., 2015; Wang and Zhao, 2016) and explaining the pattern formation mechanism in plants(Liu et al., 2010, 2011, 2013, 2015). On the other hand, the buckling of the stiff and brittle films on compliant substrates can provide large deformability for tension, compression, bending (Zhang and Chen, 2009) and other loading conditions (Ou et al., 2016). Taking advantage of this property, many kinds of stretchable electronics and devices are developed recently (Song et al., 2009; Low and Lau, 2014; Wang et al., 2015b).

According to previous study, the underlying buckling mechanism of film has been generally understood as a stress induced instability (Groenewold, 2001; Huang and Suo, 2002a, b; Chen and Hutchinson, 2004). For a stiff film bonded on a compliant substrate, there is a critical compressive stress/strain, beyond which, the film will form buckles. If the substrate is pure elastic, the critical stress/strain is constant (Huang et al., 2005; Jiang et al., 2007a, 2008a; Song et al., 2008; Cheng et al., 2014). However, if the substrate is

* Corresponding author.
E-mail address: zishunliu@mail.xjtu.edu.cn (Z. Liu).

http://dx.doi.org/10.1016/j.euromechsol.2017.08.006
0997-7538/

viscoelastic, the critical stress/strain will be changing with time and the buckling will become a kinetic process (Huang, 2005; Im and Huang, 2005; Huang and Im, 2006; Mokni et al., 2008; Jiang and Li, 2009; Chatterjee et al., 2015).

In the case of a thin film completely bonded on the compliant substrate and under a certain compressive stress/strain, the buckling geometry of the film is only determined by the relative moduli and thicknesses of the film and substrate. This phenomenon has been proved both experimentally and theoretically (Chen and Hutchinson, 2004; Song et al., 2008). To control the buckling geometry, Sun et al. (2006) developed an engineering approach to bond the Si nanoribbons partly on the PDMS substrate, and with this method, the buckling geometry could be controlled within the demanding range (Wang and Feng, 2009; Chen et al., 2011). Subsequently, Jiang et al. presented a nonlinear model to study the buckling mechanics of this type of thin film/substrate structures (Jiang et al., 2007b, 2008b).

To form different buckling patterns for thin film/substrate structures, many researchers utilize shape memory polymer (SMP) as the substrate (Fu et al., 2009; Xie et al., 2010; Zhao et al., 2011), because the shape memory effect makes it convenient to fabricate the buckling patterns. Among them, Li et al. (2012) developed an approach to create both reversible and irreversible wrinkling patterns by utilizing SMP as substrate and gold thin film as the top layer. Similar to Li's approach in creating the irreversible buckling pattern, Chen et al. (2012) developed an assisted self-assembly fabrication method using pre-programmed SMP as the substrate in the bi-layer film/substrate structure, and studied defect formation and post-buckling pattern evolution.

In this work, we study the large deformation buckling of thin films on compliant substrates and propose the buckling control method of film with the help of SMP substrate. Unlike the controlling method developed by Sun et al. (2006) who use partly bonded nanoribbons to control the buckling geometry, we use SMP as substrate to control the buckling of the thin film. The programming process is also different from the common methods which use SMP as substrate to create buckling patterns.

In our study, we consider the case of the buckling with thin films completely bonded on the compliant substrates. The schematic of buckling under consideration is illustrated in Fig. 1. First, the strain-free substrate of initial length L_0 is stretched to a nominal pre-strain of ε_{pre} (Step 1). Then, the strain-free Si film of length $(1+\varepsilon_{\text{pre}})L_0$ is bonded to the stretched substrate (Step 2). Upon releasing the pre-strain of the substrate, the buckling occurs in the film (Step 3). In all processes, it is assumed that the binding between the Si film and the substrate is strong enough without debonding.

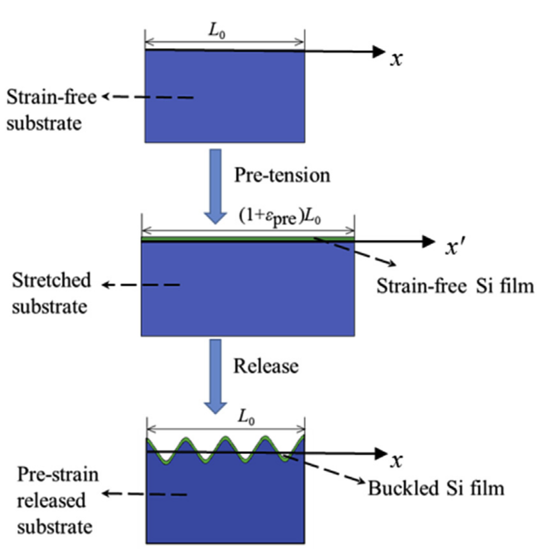

Fig. 1. Schematic of buckling of thin film on a compliant substrate.

The paper is organized as follows. First, a continuum mechanics model for the buckling of the thin film is derived based on the minimization of the total strain energy of the film/substrate system in Section 2, and the comparison with previous theories and experimental results is given. Then, a theoretical analysis and finite element simulation of the buckling property for a thin Si film on the SMP substrate are carried out in Section 3. Next, a programmed method to control the buckling of thin films on SMP substrate by take advantage of the shape memory property of the substrate is present in Section 4. Finally, the concluding remarks are given in Section 5.

2. Theoretical analysis of the buckling of film on a compliant substrate

Since the thickness of the thin film is several orders smaller than its length, the film can be treated as a beam. Because of the contraction of the substrate, the film will buckle into a wave configuration, which is schematically shown in Fig. 2. Here, the x axis is along the pre-stretched direction of the substrate and y axis is perpendicular to the surface of the substrate. To simplify the problem, plane-strain problems are considered in present analysis.

The membrane strain in the film is related to the in-plain displacement u and out-of-plane w by

$$\varepsilon = \frac{\partial u}{\partial x} + \frac{1}{2}\left(\frac{\partial w}{\partial x}\right)^2 \tag{1}$$

If the Young's modulus of the substrate E_s is much smaller than the modulus of the film E_f ($E_s \ll E_f$), the membrane strain is almost constant and much smaller than the bending strain. By assuming the membrane strain in the film is constant, Eq. (1) can be derived as

$$\frac{\partial \varepsilon}{\partial x} = \frac{\partial^2 u}{\partial x^2} + \frac{\partial w}{\partial x}\frac{\partial^2 w}{\partial x^2} = 0 \tag{2}$$

2.1. Continuum model for small deformation buckling

Assume that the out-of-plane displacement w of the buckled thin film is a cosine wrinkle with amplitude A and wavelength $\lambda = 2\pi/k$ (i.e., $w = A\cos kx$), and then the buckling geometry can be determined by a small deformation theory based method (Huang, 2005). Substituting $w = A\cos kx$ into Eq. (2), the governing equation of in-plane displacement u of the film can be expressed as

$$\frac{\partial^2 u}{\partial x^2} + A^2k^3 \sin kx \cos kx = 0 \tag{3}$$

Thus, the in-plane displacement u of the film can be obtained by solving Eq. (3)

$$u = \frac{1}{8}A^2k \sin 2\,kx + C_1x + C_2 \tag{4}$$

where the two parameters C_1 and C_2 can be determined according to the boundary conditions. By ignoring the rigid body displacement of the film, we can obtain $C_2 = 0$; by considering the continuity between the film and substrate, we can get $C_1 = -\varepsilon_{pre}$, where ε_{pre} is the pre-stretched strain applied to the substrate. Therefore, the membrane strain ε of the film can be obtained by substituting

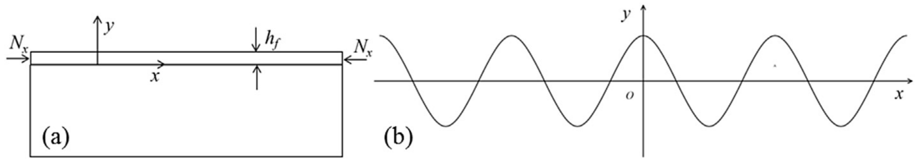

Fig. 2. (a) Schematic of film/substrate structures, (b) Schematic of the buckling of Si film.

Eq. (4) into Eq. (1)

$$\varepsilon = \frac{k^2A^2}{4} - \varepsilon_{pre} \tag{5}$$

The bending energy density (W_{b}) and the membrane energy density (W_{m}) of the film are given as following,

$$W_b = \frac{\overline{E}_f h_f^3}{24}\kappa^2 \tag{6}$$

$$W_m = \frac{\overline{E}_f h_f}{2}\varepsilon^2 \tag{7}$$

where $\kappa = w''/(1+(w')^2)^{3/2}$ is the curvature of the buckled film, w' and w'' are the first and second order derivatives of w, respectively. For small deformation, $w' \ll 1$, the approximate curvature can be obtained as $\kappa = \frac{\partial^2 w}{\partial x^2} = -Ak^2 \cos kx$.

Thus, the average bending energy (U_{b}) and membrane energy (U_{m}) for per unit length of the film, which are the integration of corresponding strain energy densities over a unit length of the thin film, can be obtained

$$U_b = \frac{1}{\lambda}\int_0^{\lambda} W_b dx = \frac{1}{\lambda}\int_0^{\lambda} \frac{\overline{E}_f h_f^3}{24}\kappa^2 dx = \frac{\pi^4 \overline{E}_f h_f^3 A^2}{3\lambda^4} \tag{8}$$

$$U_m = \frac{1}{\lambda}\int_0^{\lambda} W_m dx = \frac{1}{\lambda}\int_0^{\lambda} \frac{\overline{E}_f h_f}{2}\varepsilon^2 dx = \frac{\overline{E}_f h_f}{2}\left(\frac{\pi^2 A^2}{\lambda^2} - \varepsilon_{pre}\right)^2 \tag{9}$$

Subjecting a normal displacement $w = A\cos kx$ to the film, neglecting the shear stress on it and assuming the in-plane membrane force is $N = -\sigma_0 h_f$, according to the nonlinear Von Karman plate theory (Timoshenko, 1961), the governing equation of the film can be expressed as

$$-p = \frac{\overline{E}_f h_f}{12}\frac{\partial^4 w}{\partial x^4} - N\frac{\partial^2 w}{\partial x^2} = \left(\frac{\overline{E}_f h_f}{12}k^4 - \sigma_0 h_f k^2\right) A\cos kx \tag{10}$$

where p is the normal stress between the film and the top surface of the substrate.

The stresses in the substrate can be defined by a stress function, $\phi(x,y)$, which satisfies the following equation

$$\left(\frac{\partial^4}{\partial x^4} + 2\frac{\partial^4}{\partial x^2 \partial y^2} + \frac{\partial^4}{\partial y^4}\right)\phi = 0 \tag{11}$$

The stresses and strains at (x,y) can be determined from the stress function ϕ as follows,

$$\begin{gathered} \sigma_x = \frac{\partial^2 \phi}{\partial y^2}; \quad \sigma_y = \frac{\partial^2 \phi}{\partial x^2}; \quad \tau_{xy} = -\frac{\partial^2}{\partial x \partial y}, \\ \varepsilon_x = \frac{1-\nu_s^2}{E_s}\left(\sigma_x - \frac{\nu_s}{1-\nu_s}\sigma_y\right); \quad \varepsilon_y = \frac{1-\nu_s^2}{E_s}\left(\sigma_y - \frac{\nu_s}{1-\nu_s}\sigma_x\right) \end{gathered} \tag{12}$$

Substituting $\phi(x,y) = C_3 \cos kx(1 + C_4 y)\exp(ky)$ into Eq. (12), we can obtain the stresses and strains at the top surface ($y = 0$) of the substrate.

$$\begin{aligned} &\sigma_y = -C_3 k^2 \cos kx \\ &\varepsilon_x = -\frac{C_3 k \cos kx(1+\nu_s)(k + 2C_4 - 2C_4\nu_s)}{E_s} \end{aligned} \tag{13}$$

Since the film is only subjected with normal displacement, there are no x-displacements in the substrate. Consequently, the x-displacements and the strains ε_x at the surface are zero. Besides, the normal stress between the film and the top surface of the substrate is p. Thus, C_3 and C_4 should take the values,

$$C_3 = \frac{p}{k^2 \cos kx}, \quad C_4 = \frac{k}{2(\nu_s - 1)} \tag{14}$$

Therefore, the deflection of the top surface of the substrate δ can be obtained by integration of ε_y,

$$\begin{aligned} \delta = \int \varepsilon_y dy &= \frac{C_3 \cos kx(1+\nu_s)(k - C_4 + 2C_4\nu_s)}{E_s} \\ &= \frac{p(1+\nu_s)(3-4\nu_s)}{2E_s k(1-\nu_s)\cos kx}\cos kx = B\cos kx \end{aligned} \tag{15}$$

where $B = 2\frac{p\alpha}{\cos kx}/(\overline{E}_s k)$ with $\overline{E}_s = E_s/(1-\nu_s^2)$ is the plane-strain modulus of the substrate and $\alpha = (3-4\nu_s)/[4(1-\nu_s)^2]$ is a coefficient relating to the Poisson's ratio ν_s of the substrate (Chen and Hutchinson, 2004). Subject to $A = B$, and combine $B = 2\frac{p\alpha}{\cos kx}/(\overline{E}_s k)$ with Eq. (10), we can obtain that,

$$\sigma_0 h_f = \frac{\overline{E}_f h_f}{12}k^2 + \frac{\overline{E}_s}{2k} \tag{16}$$

$$p = \frac{\overline{E}_s k}{2\alpha}A\cos kx \tag{17}$$

For an incompressible substrate, $\nu_s = 1/2$, we can obtain that $\alpha = 1$. Thus, the energy in the substrate for per unit length can be calculated as

$$U_s = \frac{2\pi}{k}\int_0^{k/2\pi} \frac{1}{2}pwdx = \frac{\overline{E}_s k A^2}{8} = \frac{\overline{E}_s \pi A^2}{4\lambda} \tag{18}$$

The total energy of the system (thin film and thick substrate) is

$$U = U_b + U_m + U_s = \frac{\pi^4 \overline{E}_f h_f^3 A^2}{3\lambda^4} + \frac{\overline{E}_f h_f}{2}\left(\frac{\pi^2 A^2}{\lambda^2} - \varepsilon_{pre}\right)^2 + \frac{\overline{E}_s \pi A^2}{4\lambda} \tag{19}$$

By minimizing the total energy,

$$\begin{aligned}\frac{\partial U}{\partial A} &= \frac{2\pi^4 \overline{E}_f h_f^3 A}{3\lambda^4} + \overline{E}_f h_f\left(\frac{\pi^2 A^2}{\lambda^2} - \varepsilon_{pre}\right)\frac{2\pi^2 A}{\lambda^2} + \frac{\overline{E}_s \pi A}{2\lambda} \\ &= \frac{\pi A}{\lambda}\left[\frac{2\pi^3 \overline{E}_f h_f^3}{3\lambda^3} + \frac{2\pi^3 A^2 \overline{E}_f h_f}{\lambda^3} - \frac{2\pi \overline{E}_f h_f \varepsilon_{pre}}{\lambda} + \frac{\overline{E}_s}{2}\right] = 0\end{aligned} \tag{20}$$

$$\begin{aligned}\frac{\partial U}{\partial \lambda} &= \frac{-4\pi^4 \overline{E}_f h_f^3 A^2}{3\lambda^5} + \overline{E}_f h_f\left(\frac{\pi^2 A^2}{\lambda^2} - \varepsilon_{pre}\right)\frac{-2\pi^2 A^2}{\lambda^3} - \frac{\overline{E}_s \pi A^2}{4\lambda^2} \\ &= \frac{\pi A^2}{\lambda^2}\left[-\frac{4\pi^3 \overline{E}_f h_f^3}{3\lambda^3} - \frac{2\pi^3 A^2 \overline{E}_f h_f}{\lambda^3} + \frac{2\pi \overline{E}_f h_f \varepsilon_{pre}}{\lambda} - \frac{\overline{E}_s}{4}\right] = 0\end{aligned} \tag{21}$$

Eq. (20) and Eq. (21) can be simplified as follows,

$$\frac{2\pi^3 \overline{E}_f h_f^3}{3\lambda^3} + \frac{2\pi^3 A^2 \overline{E}_f h_f}{\lambda^3} - \frac{2\pi \overline{E}_f h_f \varepsilon_{pre}}{\lambda} + \frac{\overline{E}_s}{2} = 0 \tag{22}$$

$$-\frac{4\pi^3 \overline{E}_f h_f^3}{3\lambda^3} - \frac{2\pi^3 A^2 \overline{E}_f h_f}{\lambda^3} + \frac{2\pi \overline{E}_f h_f \varepsilon_{pre}}{\lambda} - \frac{\overline{E}_s}{4} = 0 \tag{23}$$

Adding Eq. (22) and Eq. (23) together, we can obtain

$$-\frac{2\pi^3 h_f^3 \overline{E}_f}{3\lambda^3} + \frac{\overline{E}_s}{4} = 0 \tag{24}$$

Thus, based on small deformation theory, the wavelength λ_0 can be calculated and the amplitude A_0 can be obtained subsequently as follows,

$$\lambda_0 = 2\pi h_f \left(\frac{\overline{E}_f}{3\overline{E}_s}\right)^{\frac{1}{3}} \tag{25}$$

$$A_0 = h_f \sqrt{\frac{\varepsilon_{pre}}{\varepsilon_c} - 1} \tag{26}$$

where $\varepsilon_c = \frac{1}{4}(3\overline{E}_s/\overline{E}_f)^{\frac{2}{3}}$ is the critical buckling strain.

2.2. Continuum model for finite deformation buckling

Jiang et al. (2007a) and Song et al. (2008) pointed out that the wavelength is strain-dependent. The continuum model of buckling based on small deformation cannot predict well for the finite deformation buckling. Thus, it is necessary to develop the continuum model for buckling based on finite deformation.

2.2.1. Review of previous continuum models for finite deformation

To predict the buckling geometry for finite deformation, Jiang et al. (2007a) established a large deformation buckling theory. In here, for the sake of simplicity, we will briefly introduce the derivation steps.

First, the out-of-plane displacement w of the buckled thin film is represented by

$$w = A\cos\frac{2\pi x}{\lambda} = A\cos\frac{2\pi x'}{(1+\varepsilon_{pre})\lambda} \tag{27}$$

where the coordinate x' in the substrate-stretched configuration and the x in the substrate-strain-free configuration are related by $x' = (1+\varepsilon_{pre})x$, which can be obtained from Fig. 1.

Thus, the bending energy U_b and membrane energy U_m in the film for per unit length are revised by replacing the coordinate x to x' in Eqs. (8) and (9) as follows,

$$U_b = \frac{\pi^4 \overline{E}_f h_f^3 A^2}{3\lambda^4 (1+\varepsilon_{pre})^4} \tag{28}$$

$$U_m = \frac{\overline{E}_f h_f}{2}\left(\frac{\pi^2 A^2}{\lambda^2 (1+\varepsilon_{pre})^2} - \frac{\varepsilon_{pre}}{1+\varepsilon_{pre}}\right)^2 \tag{29}$$

Then, the energy in the substrate for per unit length U_s is derived using perturbation method to be (Song et al., 2008),

$$U_s = \frac{\overline{E}_s \pi A^2}{3\lambda(1+\varepsilon_{pre})}\left(1 + \frac{5}{32}\frac{\pi^2 A^2}{\lambda^2}\right) \tag{30}$$

Therefore, the total energy per unit length of the film/subtract system is obtained as

$$\begin{aligned}U &= U_b + U_m + U_s \\ &= \frac{\pi^4 \overline{E}_f h_f^3 A^2}{3\lambda^4 (1+\varepsilon_{pre})^4} + \frac{\overline{E}_f h_f}{2}\left(\frac{\pi^2 A^2}{\lambda^2 (1+\varepsilon_{pre})^2} - \frac{\varepsilon_{pre}}{1+\varepsilon_{pre}}\right)^2 \\ &\quad + \frac{\overline{E}_s \pi A^2}{3\lambda(1+\varepsilon_{pre})}\left(1 + \frac{5}{32}\frac{\pi^2 A^2}{\lambda^2}\right)\end{aligned} \tag{31}$$

By minimizing the total energy, $\partial U/\partial A = \partial U/\partial\lambda = 0$, the wavelength λ and amplitude A can be obtained as follows,

$$\lambda = \frac{2\pi h_f}{(1+\varepsilon_{pre})(1+\xi)^{1/3}}\left(\frac{\overline{E}_f}{3\overline{E}_s}\right)^{\frac{1}{3}} = \frac{\lambda_0}{(1+\varepsilon_{pre})(1+\xi)^{1/3}} \tag{32}$$

$$A \approx \frac{A_0}{\sqrt{1+\varepsilon_{pre}}(1+\xi)^{1/3}} \tag{33}$$

where λ_0 and A_0 are the wavelength and amplitude in Eqs. (25) and (26) based on the small deformation theory, and $\xi = 5\varepsilon_{pre}(1+\varepsilon_{pre})/32$.

By adopting a similar process, Cheng and Song (2013) developed a simple theory to determine the buckling geometry in finite deformation. Instead of the complex expression given by Song et al. (2008), the energy per unit length in the substrate U_s is also obtained by replacing the coordinate x to x' as the bending energy U_b and membrane energy U_m in the film, which is

$$U_s = \frac{\overline{E}_s \pi A^2}{4\lambda(1+\varepsilon_{pre})} \tag{34}$$

Combining Eqs. (28), (29) and (34), the total energy per unit length is obtained as

$$U = U_b + U_m + U_s = \frac{\pi^4 \overline{E}_f h_f^3 A^2}{3\lambda^4 (1+\varepsilon_{pre})^4} + \frac{\overline{E}_f h_f}{2}\left(\frac{\pi^2 A^2}{\lambda^2 (1+\varepsilon_{pre})^2} - \frac{\varepsilon_{pre}}{1+\varepsilon_{pre}}\right)^2 + \frac{\overline{E}_s \pi A^2}{4\lambda(1+\varepsilon_{pre})} \tag{35}$$

By minimizing the total energy,

$$\frac{\partial U}{\partial A} = \frac{2\pi^4 \overline{E}_f h_f^3 A}{3\lambda^4 (1+\varepsilon_{pre})^3} L_0 + \overline{E}_f h_f \left(\frac{\pi^2 A^2}{\lambda^2 (1+\varepsilon_{pre})^2} - \frac{\varepsilon_{pre}}{1+\varepsilon_{pre}}\right) \frac{2\pi^2 A}{\lambda^2 (1+\varepsilon_{pre})^2}(1+\varepsilon_{pre}) L_0 + \frac{\overline{E}_s \pi A}{2\lambda} L_0 = \frac{\pi A L_0}{\lambda}\left[\frac{2\pi^3 \overline{E}_f h_f^3}{3\lambda^3 (1+\varepsilon_{pre})^3} + \frac{2\pi^3 A^2 \overline{E}_f h_f}{\lambda^3 (1+\varepsilon_{pre})^3} - \frac{2\pi \overline{E}_f h_f \varepsilon_{pre}}{\lambda (1+\varepsilon_{pre})^2} + \frac{\overline{E}_s}{2}\right] = 0 \tag{36}$$

$$\frac{\partial U}{\partial \lambda} = \frac{-4\pi^4 \overline{E}_f h_f^3 A^2}{3\lambda^5 (1+\varepsilon_{pre})^3} L_0 + \overline{E}_f h_f \left(\frac{\pi^2 A^2}{\lambda^2 (1+\varepsilon_{pre})^2} - \frac{\varepsilon_{pre}}{1+\varepsilon_{pre}}\right) \frac{-2\pi^2 A^2}{\lambda^3 (1+\varepsilon_{pre})^2}(1+\varepsilon_{pre}) L_0 - \frac{\overline{E}_s \pi A^2}{4\lambda^2} L_0 = \frac{\pi A^2 L_0}{\lambda^2}\left[-\frac{4\pi^3 \overline{E}_f h_f^3}{3\lambda^3 (1+\varepsilon_{pre})^3} - \frac{2\pi^3 A^2 \overline{E}_f h_f}{\lambda^3 (1+\varepsilon_{pre})^3} + \frac{2\pi \overline{E}_f h_f \varepsilon_{pre}}{\lambda (1+\varepsilon_{pre})^2} - \frac{\overline{E}_s}{4}\right] = 0 \tag{37}$$

Eqs. (36) and (37) can be simplified as follows,

$$\frac{2\pi^3 \overline{E}_f h_f^3}{3\lambda^3 (1+\varepsilon_{pre})^3} + \frac{2\pi^3 A^2 \overline{E}_f h_f}{\lambda^3 (1+\varepsilon_{pre})^3} - \frac{2\pi \overline{E}_f h_f \varepsilon_{pre}}{\lambda (1+\varepsilon_{pre})^2} + \frac{\overline{E}_s}{2} = 0 \tag{38}$$

$$-\frac{4\pi^3 \overline{E}_f h_f^3}{3\lambda^3 (1+\varepsilon_{pre})^3} - \frac{2\pi^3 A^2 \overline{E}_f h_f}{\lambda^3 (1+\varepsilon_{pre})^3} + \frac{2\pi \overline{E}_f h_f \varepsilon_{pre}}{\lambda (1+\varepsilon_{pre})^2} - \frac{\overline{E}_s}{4} = 0 \tag{39}$$

Adding Eqs. (38) and (39) together, we can obtain

$$-\frac{2\pi^3 h_f^3 \overline{E}_f}{3\lambda^3 (1+\varepsilon_{pre})^3} + \frac{\overline{E}_s}{4} = 0 \tag{40}$$

Thus, the wavelength λ can be calculated out and the amplitude A can be obtained subsequently as follows,

$$\lambda = \frac{2\pi h_f}{1+\varepsilon_{pre}}\left(\frac{\overline{E}_f}{3\overline{E}_s}\right)^{\frac{1}{3}} = \frac{\lambda_0}{1+\varepsilon_{pre}} \tag{41}$$

$$A = h_f \sqrt{\frac{\varepsilon_{pre}}{\varepsilon_c (1+\varepsilon_{pre})} - 1} \tag{42}$$

where $\varepsilon_c = \frac{1}{4}(3\overline{E}_s/\overline{E}_f)^{\frac{2}{3}}$ is the critical buckling strain.

2.2.2. Improved continuum model for finite deformation

As we know, the analytical solution for the curvature of a curve is $\kappa = w''/(1+(w')^2)^{3/2}$ (Chen et al., 2016), and for small deformation, $w' \ll 1$, the curvature is approximately taken as $\kappa = w'' = \frac{\partial^2 w}{\partial x^2}$. This approximation is also adopted in previous large deformation continuum theory for the buckling of thin film on the compliant substrate. However, through extensive study for the theoretical analyses, we find that there is a significant difference in obtained results with and without this approximation. The continuum model considering precise curvature of the buckled film for large deformation buckling is derived based on Cheng and Song (2013). Besides, we also include the effect of the Poisson's ratio of the substrate, because the Poisson's ratio of SMP substrate is changing with temperature and cannot always be treated as incompressible in our extended study.

By taking the precise form, the curvature of the buckled film can be obtain as

$$\kappa = \frac{-Ak^2 \cos kx}{(1+A^2k^2 \sin^2 kx)^{3/2}} = \frac{-\frac{Ak^2}{(1+\varepsilon_{pre})^2}\cos\frac{kx'}{1+\varepsilon_{pre}}}{\left(1+\frac{A^2k^2}{(1+\varepsilon_{pre})^2}\sin^2\frac{kx'}{1+\varepsilon_{pre}}\right)^{3/2}} \tag{43}$$

Thus, the bending energy U_b in the film for per unit length with coordinate x' can be determined as follows,

$$U_b = \frac{1}{\lambda}\int_0^{\lambda} \frac{\overline{E}_f h_f^3}{24}\kappa^2 dx' = \frac{\overline{E}_f h_f^3 A^2 k^4}{48(1+\varepsilon_{pre})^4}\beta \tag{44}$$

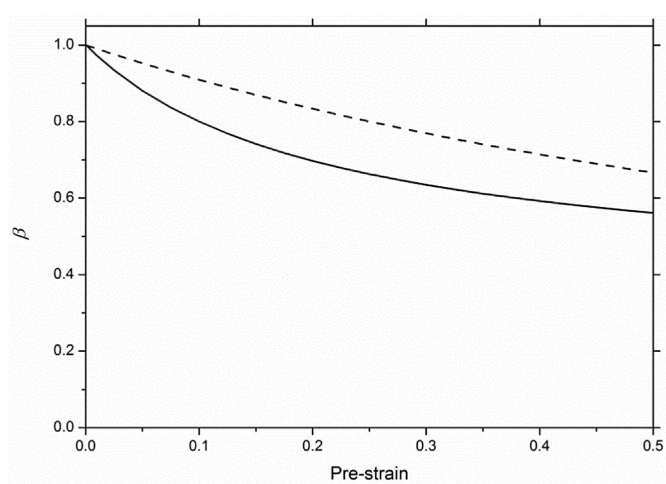

Fig. 3. The value of β as a function of pre-strain applied to the substrate, the solid line represents $\beta = \left[1+\frac{3}{4}A^2k^2/(1+\varepsilon_{pre})^2\right]\Big/[1+A^2k^2/(1+\varepsilon_{pre})^2]^{3/2}$, where the values of A and $k = 2\pi/\lambda$ are calculated based on the theory developed by Song et al. (2008), and the dash line represents the simplified form of $\beta = 1/(1+\varepsilon_{pre}-\varepsilon_c^{true})$.

where $\beta = \left[1+\frac{3}{4}A^2k^2/(1+\varepsilon_{pre})^2\right] \Big/ [1+A^2k^2/(1+\varepsilon_{pre})^2]^{3/2}$.

Compared Eq. (44) with Eq. (28), we can find that these two bending energy are equal only when $\beta = 1$. However, as the pre-strain ε_{pre} increases, the value of β becomes smaller and smaller as shown in Fig. 3, which cannot be treated as a constant of one. Therefore, it is necessary to adopt the precise curvature of the film for large deformation buckling.

The membrane energy U_m (per unit length) in the film is the same as Eq. (29) given by Cheng and Song (2013), substituting $\lambda = 2\pi/k$, we can obtain

$$U_m = \frac{\overline{E}_f h_f}{2}\left(\frac{k^2A^2}{4(1+\varepsilon_{pre})^2} - \frac{\varepsilon_{pre}}{1+\varepsilon_{pre}}\right)^2 \tag{45}$$

Considering a compressible substrate, with Eqs. (17) and (18), we can obtain the energy in the substrate U_s (per unit length) as

$$U_s = \frac{2\pi}{k}\int_0^{k/2\pi} \frac{1}{2}pwdx' = \frac{\overline{E}_s kA^2}{8\alpha(1+\varepsilon_{pre})} \tag{46}$$

where $\alpha = (3-4\nu_s)/[4(1-\nu_s)^2]$.

The total energy of the system (thin film and thick substrate) is

$$\begin{aligned} U &= U_b + U_m + U_s \\ &= \frac{\overline{E}_f h_f^3 A^2 k^4}{48(1+\varepsilon_{pre})^4}\beta + \frac{\overline{E}_f h_f}{2}\left(\frac{k^2A^2}{4(1+\varepsilon_{pre})^2} - \frac{\varepsilon_{pre}}{1+\varepsilon_{pre}}\right)^2 + \frac{\overline{E}_s kA^2}{8\alpha(1+\varepsilon_{pre})} \end{aligned} \tag{47}$$

By minimizing the total energy, $\partial U/\partial k = \partial U/\partial A = 0$, we can obtain the wavelength λ and amplitude A as following,

$$\begin{aligned} \lambda &= \frac{2\pi}{k} \\ &= \frac{\lambda_0\alpha^{1/3}}{(1+\varepsilon_{pre})}\left(1+\frac{3A^2\pi^2}{\lambda^2(1+\varepsilon_{pre})^2}\right)^{1/3} \Big/ \left(1+\frac{4A^2\pi^2}{\lambda^2(1+\varepsilon_{pre})^2}\right)^{1/2} \\ &= \frac{\lambda_0(\alpha\beta)^{1/3}}{(1+\varepsilon_{pre})} \end{aligned} \tag{48}$$

$$A = h_f\sqrt{\frac{\beta^{2/3}\varepsilon_{pre}}{(1+\varepsilon_{pre})\varepsilon_c} - \beta\left(\frac{4A^4\pi^4}{\lambda^4(1+\varepsilon_{pre})^4} + \frac{3A^2\pi^2}{\lambda^2(1+\varepsilon_{pre})^2} + 1\right) \Big/ \left(\frac{4A^2\pi^2}{\lambda^2(1+\varepsilon_{pre})^2} + 1\right)} \tag{49}$$

where λ_0 is the wavelength of small deformation buckling in Eq. (25), $\alpha = (3-4\nu_s)/[4(1-\nu_s)^2]$, $\beta = \left[1+\frac{3}{4}A^2k^2/(1+\varepsilon_{pre})^2\right] \Big/ [1+A^2k^2/(1+\varepsilon_{pre})^2]^{3/2}$ and the corresponding critical buckling strain is $\varepsilon_c = \frac{1}{4}[3\overline{E}_s/(\overline{E}_f\alpha)]^{\frac{2}{3}}$.

With Eqs. (48) and (49), the wavelength $\lambda = 2\pi/k$ and amplitude A for different pre-strains can be obtained using numerical iterative method with any initial values of amplitudes and non-zero wavelengths (such as λ_0 and A_0).

However, we find that the true critical buckling strain ε_c^{true} is larger than ε_c. Considering the critical buckling condition (when the pre-strain is equal to the true critical buckling strain, $\varepsilon_{pre} = \varepsilon_c^{true}$), the buckling amplitude $A = 0$ and $\beta = 1$. Substituting these equations into Eq. (49), we could obtain the true critical buckling strain as follows,

$$\varepsilon_c^{true} = \frac{\varepsilon_c}{1-\varepsilon_c} \tag{50}$$

2.3. Results and discussion

To validate the effectiveness of the proposed finite deformation model for buckling of thin film on compliant substrate, we adopt the literature values for the mechanical properties of Si film on PDMS substrate ($E_f = 130$ GPa, $\nu_f = 0.27$, $h_f = 100$ nm, $E_s = 1.8$ MPa, $\nu_s = 0.48$). The theoretical results are calculated based on different theories and compared with the experimental results taken from Jiang et al. (2007a), as shown in Fig. 4.

From Fig. 4, we can obtain the following conclusions. First, we will get a lower value of wavelength for the large deformation buckling to consider the precise curvature than the approximate curvature of the film. From Fig. 4(a), it can be seen that the wavelength obtained from present theory (the red line) is lower than the experimental results. This may be caused by the imperfection method in energy calculation and the viscoelasticity of the substrate (the properties of PDMS are also time-dependent, which has been proved by previous experiments (Kim et al., 2008)). The effect of viscoelasticity will be studied in more details in the next section, and the wavelength will decreases as time increases. From Fig. 4(b), it can be observed that present theory, which considers the precise curvature of the film and the Poisson's ratio of the substrate, gives a more accurate result of amplitude for the large deformation buckling. Furthermore, it can be found that the predictive wavelength by the present theory is dependent on the pre-strain, and λ approaches to λ_0 for small strain.

Since the expressions of the wavelength and amplitude in present theory are very complicated, we make a modification for the theory to give a more accurate prediction for large deformation buckling. To simplify the expressions of the wavelength and amplitude, we decide to give a concise form of β. Considering that β should satisfy the critical buckling condition ($A = 0$ and $\beta = 1$ for $\varepsilon_{pre} = \varepsilon_c^{true}$), we give $\beta = 1/(1+\varepsilon_{pre}-\varepsilon_c^{true})$ as shown in Fig. 3. Then, by substituting β into Eq. (44), we can obtain the bending energy U_b (per unit length) in the film as follows,

$$U_b = \frac{\overline{E}_f h_f^3 A^2 k^4}{48(1+\varepsilon_{pre})^4}\beta = \frac{\overline{E}_f h_f^3 A^2 k^4}{48(1+\varepsilon_{pre})^4}\frac{1}{1+\varepsilon_{pre}-\varepsilon_c^{true}} \tag{51}$$

Combining Eq. (51) with (45) and (46), by minimizing the total energy $U = U_b + U_m + U_s$, we can obtain the wavelength λ and amplitude A as following,

$$\lambda = \frac{\lambda_0}{1+\varepsilon_{pre}}(\alpha\beta)^{1/3} \tag{52}$$

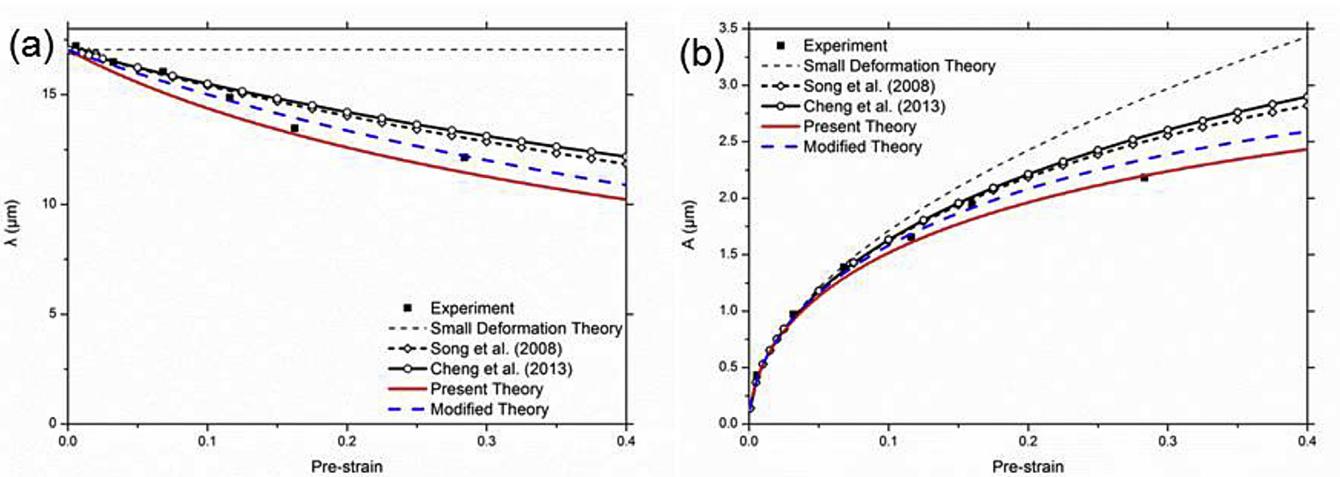

Fig. 4. (a) Wavelength and (b) Amplitude of buckled Si film (100 nm thickness) on PDMS substrate as a function of pre-strain. The red line (Present Theory) is corresponding to Eqs. (48) and (49). The blue dash lines (Modified Theory) are the modified model corresponding to Eqs. (52) and (53). (For interpretation of the references to colour in this figure legend, the reader is referred to the web version of this article.)

$$A = h_f\sqrt{\frac{\beta^{2/3}\varepsilon_{pre}}{\varepsilon_c(1+\varepsilon_{pre})} - \beta} \tag{53}$$

where λ_0 is the wavelength in Eq. (25), $\varepsilon_c = \frac{1}{4}[3\overline{E}_s/(\overline{E}_f\alpha)]^{\frac{2}{3}}$ is the critical buckling strain and $\beta = 1/(1+\varepsilon_{pre} - \varepsilon_c^{true})$.

Eq. (52) and Eq. (53) forms the modified theory for large deformation buckling. The predictive wavelengths and amplitudes with this modified theory for finite pre-strain also agree well with the experimental results, as shown in Fig. 4 (the blue dash line).

3. Buckling behavior of elastic films on SMP substrate

This section will deal with the buckling behavior of Si films on SMP substrates. First, we give an introduction of the material and the theory to model the SMP substrate. Then, a theoretical analysis of the buckling behavior is carried out. Finally, the time-dependent evolution process of the buckling geometry is studied theoretically and finite element simulations are carried out to validate the theoretical analysis.

3.1. SMP substrate model and assumption

In present study, the SMP substrate is a kind of epoxy polymers named epoxy 12DA3. To describe the mechanical properties of this SMP substrate, the generalized Maxwell model as shown in Fig. 5 is adopted.

The detailed descriptions and derivation process for this model have already been presented in the reference (He et al., 2015), and here we just give some essential equations.

The basic hereditary integral formulation for linear isotropic viscoelasticity is

$$\boldsymbol{\sigma}(t) = \int_0^t 2G(\tau-\tau')\dot{\mathbf{e}}dt' + \mathbf{I}\int_0^t K(\tau-\tau')\dot{\phi}dt' \tag{54}$$

where $\boldsymbol{\sigma}$ is the instantaneous Caughy stress, $\mathbf{e}$ and ϕ are the mechanical deviatoric and volumetric strains, '·' denotes differentiation with respect to t', K and G are the time-dependent small-strain shear and bulk relaxation moduli, which are functions of the reduced time τ,

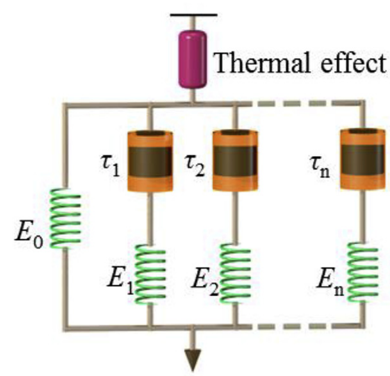

Fig. 5. Generalized Maxwell model.

Using integration by parts and a variable transformation, Eq. (54) can be written in the form as follows,

$$\boldsymbol{\sigma}(t) = 2G_0\mathbf{e}(t) + \int_0^\tau 2\dot{G}(\tau')\mathbf{e}(t-t')d\tau' + \mathbf{I}\left(K_0\phi(t) + \int_0^\tau \dot{K}(\tau')\phi(t-t')d\tau'\right) \tag{55}$$

where G_0 and K_0 are the instantaneous small strain shear and bulk moduli. $\dot{G}(\tau') = dG(\tau')/d\tau'$, and $\dot{K}(\tau') = dK(\tau')/d\tau'$. For the non-isothermal process, recall that the reduced time τ represents a shift in time with temperature

$$\frac{d\tau}{dt} = \frac{1}{a_T(T(t))} \tag{56}$$

where $a_T(T)$ is the time-temperature superposition shifting factor following the classic Williams-Landel-Ferry (WLF) equation,

$$\lg(a_T) = \frac{-C_1\left(T - T_{ref}\right)}{C_2 + T - T_{ref}} \quad (57)$$

where C_1 and C_2 are material constants. T_{ref} is the WLF reference temperature. According to Diani et al., the parameters are taken as $C_1 = 10.17$, $C_2 = 47.35$ °C, $T_{ref} = 50$ °C.

In constitutive Eq. (55), the bulk modulus can be treated as a constant value, while the relaxation shear moduli $G(t)$ can be expressed in terms of Prony series,

$$G(\tau) = G_\infty + \sum_{i=1}^{n} G_i e^{-\tau/\tau_i} \quad (58)$$

where $G_\infty = 1.6$ MPa represent the shear moduli at time $t = \infty$. n is taken as 12 in Diani et al. (2012), and τ_i and G_i ($i = 1, 2 \ldots 12$) are series of relaxation times and relaxation moduli respectively; their values are listed in Table 1 and the bulk modulus of the material is taken as a constant value $K = 3.1$ GPa.

As we all know, considering the time-temperature equivalence principle, the glassy state at low temperature and rubbery state at high temperature for viscoelastic materials are equivalent to the material properties at $t = 0+$ and $t = \infty$, respectively. Thus, for the SMP in this study, we will take the glassy state (30 °C) and rubbery state (70 °C) to represent the properties at $t = 0+$ and $t = \infty$, and the state at an intermediate temperature (30 °C–70 °C) to represent the properties after relaxation for a time t. Here, the mechanical properties (Young's modulus and Poisson's ratio) at different temperatures are all taken the value after relaxation for 1s.

At the reference temperature $T_{ref} = 50$ °C, substituting the constant bulk modulus and the relaxation shear modulus into $\nu_s = \frac{1}{2}(3K - 2G)/(3K + G)$, we can obtain the Poisson's ratio $\nu_s(t)$, which is a function of relaxation time t, as shown in Fig. 6(a), and it can cover the Poisson's ratio both at glassy state $\nu_s(0) = \nu_{s0} \approx 0.38$ and at rubbery state as $\nu_s(\infty) = \nu_{s\infty} \approx 0.5$. Furthermore, considering $E_s = 2G(1 + \nu_s)$, the relaxation Young's modulus $E_s(t)$ at $T_{ref} = 50$ °C can be expressed as a function of time as shown in Fig. 6(b).

The buckling process of thin film on SMP substrate is hardly reaching equilibrium unless the SMP substrate is in the rubbery state. This phenomenon have been observed from previous study about the buckling of thin film on viscoelastic substrate (Huang and Suo, 2002a, b; Huang et al., 2004; Huang, 2005; Im and Huang, 2005; Huang and Im, 2006; Jiang and Li, 2009) and will be explained in finite element simulation in section 4. However, during the theoretical analysis, we make an assumption that the buckling occurs instantaneously, which means that the buckling is always in the equilibrium state and the mechanical properties (Young's modulus and Poisson's ratio) will not change during the buckling, thus we can obtain the expected buckling geometry at any temperature and time. Although the expected buckling geometry may not be easily observed in real experiment and it could not completely reflect the evolution process of buckling, it can give us a better understanding that the evolution of buckling does exist and the wavelength and amplitude are changing continually as time or temperature changes for the SMP substrate.

To validate the correctness of the calculation and simulation results based on this assumption, we refers to the buckling experiments of thin Al film on SMP substrate with different film thicknesses reported by Chen et al. (2012). In their study, the experiments were carried out to investigate the influence of film thickness on the buckling geometry. The substrate was an epoxy resin-based SMP reported by Xie et al. (2010), and was programmed with 2.9% pre-strain at a high temperature. The thin Al films with different thicknesses form 10 nm–60 nm were then deposited at different places on the same piece of substrate after fixed by cooling, and finally the buckling occurred during the substrate strain recovery process by heating. The experimental results of the buckling geometry of the thin Al film are also depicted in Fig. 7.

Table 1
Generalized Maxwell model relaxation times and associated shear moduli pairs (Diani et al., 2012).

τ_i(s)	0.3031×10^{-4}	0.1721×10^{-3}	0.9768×10^{-3}	0.5545×10^{-2}	0.3147×10^{-1}	0.1787
G_i(Pa)	0.1476×10^{9}	0.1756×10^{9}	0.2025×10^{9}	0.1775×10^{9}	0.6802×10^{8}	0.1139×10^{8}
τ_i(s)	0.1014×10^{1}	0.5757×10^{1}	0.3268×10^{2}	0.1855×10^{3}	0.1053×10^{4}	0.5977×10^{4}
G_i(Pa)	0.2264×10^{7}	0.8132×10^{6}	0.4020×10^{6}	0.1760×10^{6}	0.5056×10^{5}	0.1265×10^{5}

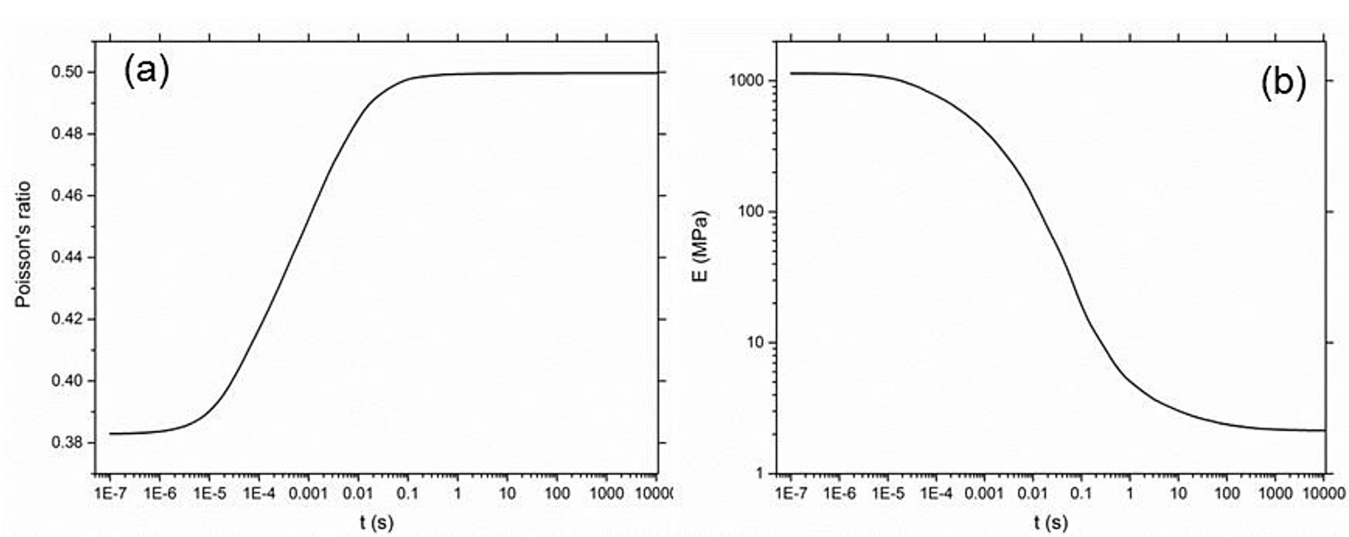

Fig. 6. (a) Poisson's ratio and (b) Relaxation Young's modulus as a function of time for the substrate at a temperature of 50 °C.

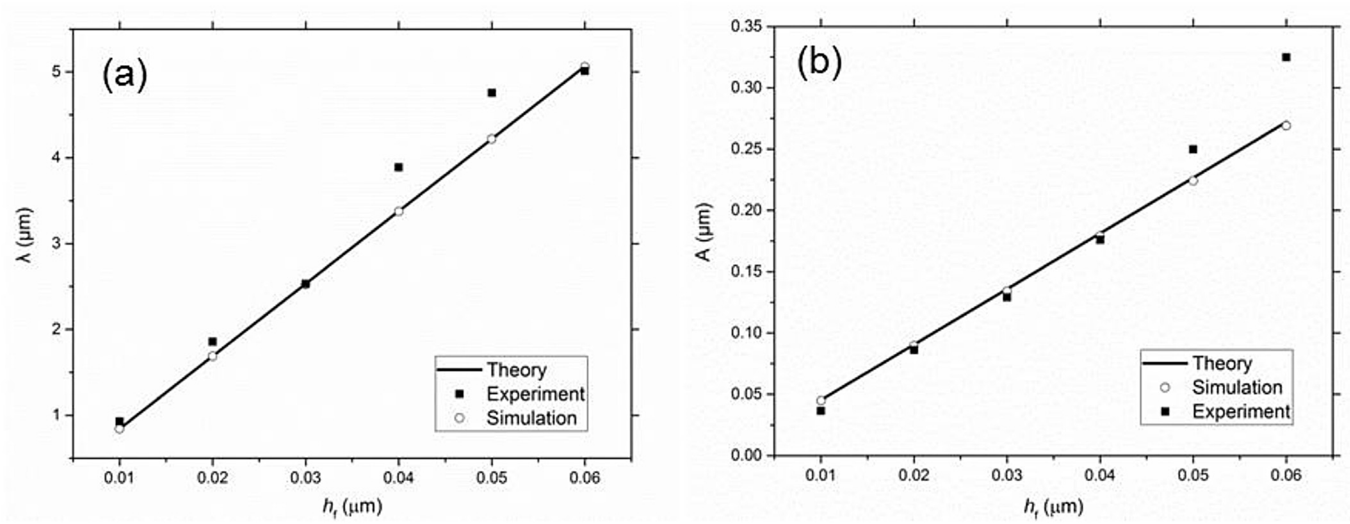

Fig. 7. (a) Wavelength and (b) Amplitude vs thickness of Al film on the 2.9% pre-strain SMP substrate.

To perform FEM simulation and theoretical analysis, the Young's modulus and Poisson's ratio of the SMP substrate are taken as $E_s = 8.0$ MPa and $\nu_s = 0.45$ which are the mechanical parameters in rubbery state (Chen et al., 2012), and the Young's modulus and Poisson's ratio of the thin Al film are taken as $E_f = 70$ GPa and $\nu_f = 0.346$. The simulation results and theoretical prediction are plotted as the hollow dots and solid line in Fig. 7, respectively. From the comparison with the experimental results, we can find that the theoretical prediction and FEM simulation results based on the assumption works quite well. Thus, all the following theoretical analysis and simulations in this section will adopt this assumption that the buckling occurs instantaneously.

3.2. Temperature influence

Since SMP is a kind of time and temperature dependent material, the buckling of thin Si film on SMP substrate may also be influenced by different temperatures and relaxation times. This section will focus on the influence of temperature on the buckling property. The Young's moduli and Poisson's ratios for different states are taken as the corresponding values after relaxation for 1s based on previous assumption. For the model, the thickness of the thin Si film is taken as 100 nm. With the help of the large deformation theory (Eq. (48)–(49)) proposed in Section 2.2.2, we can determine the wavelengths and amplitudes at different temperatures after releasing the various pre-strains prescribed in the substrate, and the analytical results are shown in Fig. 8.

From Fig. 8 (a) and (b), we can find that, with a larger pre-strain, the wavelength is smaller and the amplitude is larger in the temperature range considered. Besides, for each line with a certain pre-strain, the wavelength and the amplitude are increasing as the temperature increases. The increasing rate changes fast between 35 °C and 50 °C, while it is almost constant below 35 °C and above 50 °C. This temperature range is consistent with the glass transition temperature range of the SMP substrate as shown in Fig. 8 (c), the changing of Poisson's ratio is also prominent in this temperature range as shown in Fig. 8 (d).

According to the above analysis, we have learnt that the buckling geometry changes significantly in the temperature range from 35 °C to 50 °C. Thus, in the study, six temperature values are chosen to represent the different states of the substrate: 30 °C for the glassy state, 70 °C for the rubbery state, and the other temperatures (35 °C, 40 °C, 45 °C and 50 °C) for the intermediate states. With the help of the modified theory, we can obtain the amplitudes after releasing the different pre-strains given to the substrate, and the analytical results are shown in Fig. 9. In the Fig. 9, the red and blue solid lines represent the amplitudes at the rubbery state and glassy state, respectively. The dash lines represent the expected amplitudes in the intermediate states. The intersections of the lines and strain axis represent the critical buckling strains at different states, and the buckling will take place (the amplitude is no longer zero) only when the pre-strain is larger than the critical buckling strain.

From Fig. 9, we find that the two critical buckling strains ε_{c0} at glassy state and $\varepsilon_{c\infty}$ at rubbery state divide the pre-strain into three types, and thus the buckling of the film will present three different phenomena. First, if the pre-strain of the substrate is very small ($\varepsilon_{pre} < \varepsilon_{c\infty}$), the flat film is stable at both the glassy and rubbery states, and the buckling will not occur at all. Second, if the pre-strain of the substrate is quite large ($\varepsilon_{pre} > \varepsilon_{c0}$), the film will buckles immediately at the glassy state and reaches equilibrium, and the equilibrium amplitude is shown as the blue line in Fig. 9; But then the substrate will soften and change from glassy state to rubbery state as time goes on, and the buckling will evolve accordingly; Thus, the buckling will finally reaches equilibrium when the substrate is at its rubbery state after a long enough period of time. Third, if the pre-strain is between the two critical values ($\varepsilon_{c\infty} < \varepsilon_{pre} < \varepsilon_{c0}$), the flat film will start to grow buckling without experiencing the equilibrium at glassy state, and finally reach equilibrium when the substrate becomes rubbery as time goes on. The buckling evolution will be studied in detail in Section 3.4.

3.3. Time influence

To study the time-dependent behavior of buckling properties of the thin Si film on the SMP substrate, we collect the critical buckling strains after the SMP substrate relaxed for different period of time at a temperature of 70 °C, 50 °C, 45 °C, 40 °C, 35 °C and 30 °C, respectively. The critical buckling strains as a function of relaxation time are plotted in Fig. 10.

From Fig. 10, we can find that the critical buckling strain is lower at a higher temperature, which can also be observed in Fig. 9. Besides, the critical buckling strains are time-dependent. With a longer relaxation time, the critical buckling strain will keep on decreasing unless it reaches a minimum value $\varepsilon_{c\infty}$. This is because

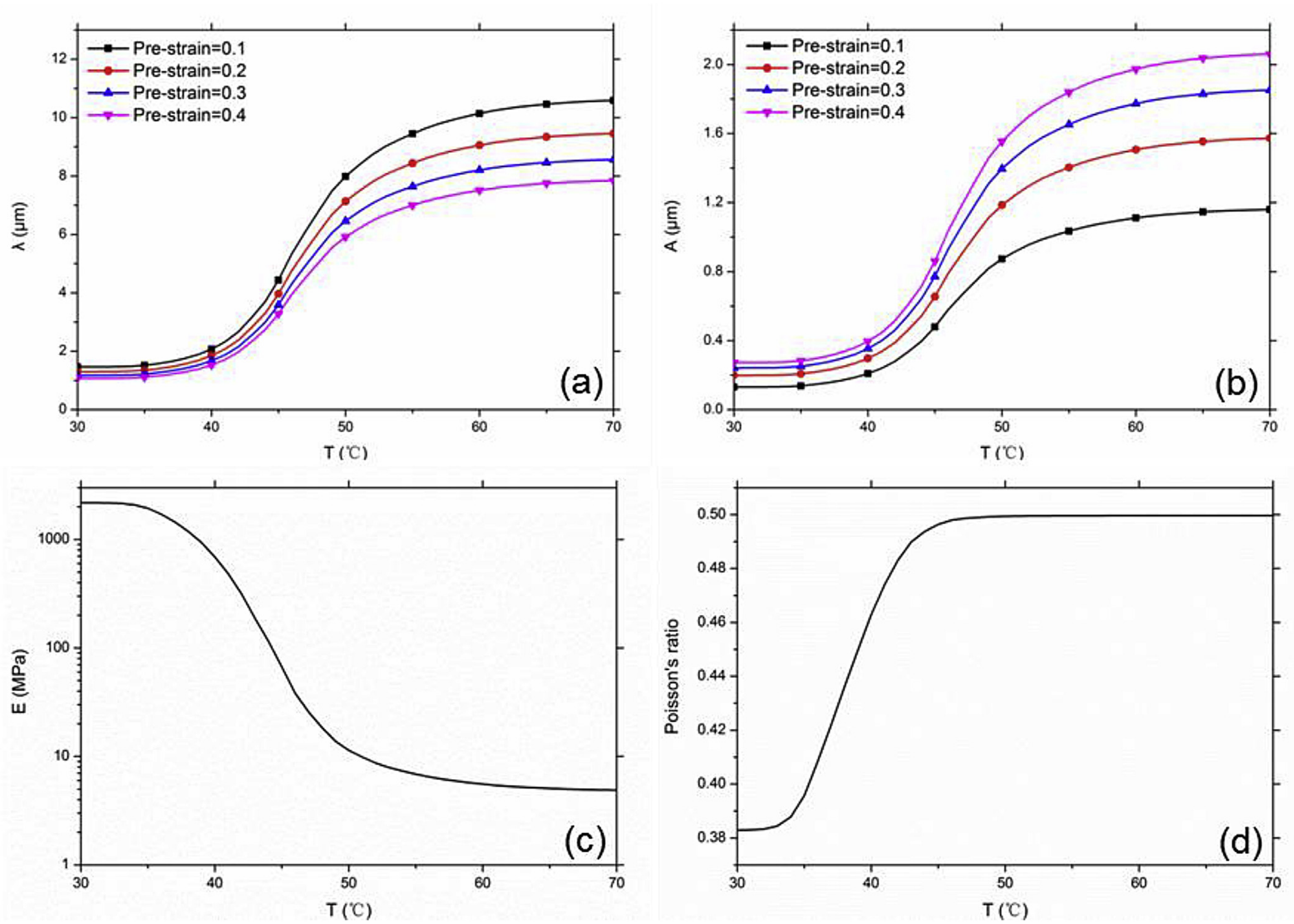

Fig. 8. (a) Wavelength and (b) Amplitude of Si film on SMP substrate as a function of temperature with different pre-strains. (c) Instantaneous Young's modulus and (d) Poisson's ratio of the SMP substrate as a function of temperature.

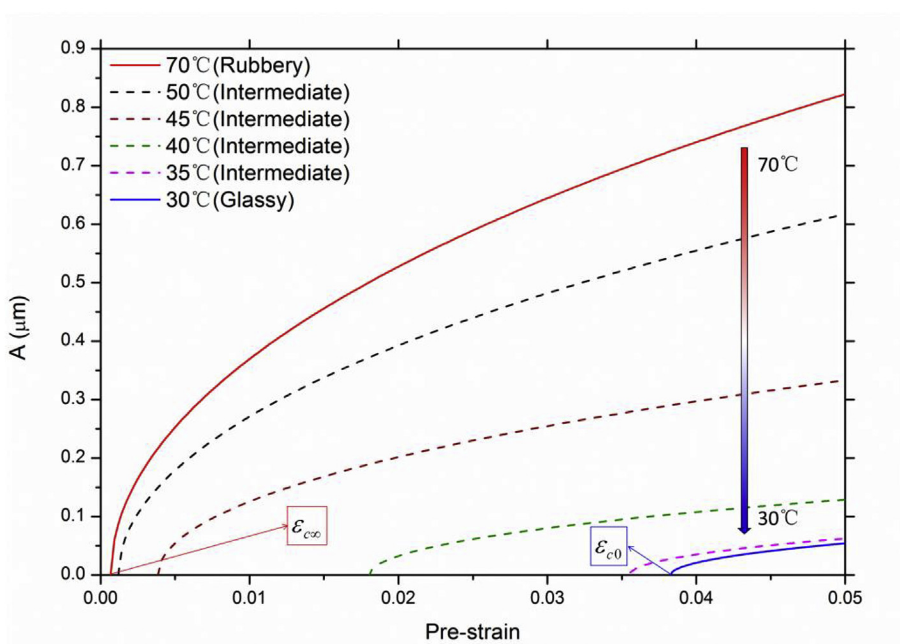

Fig. 9. Buckling amplitudes of thin Si films on SMP substrates of different states. The red and blue solid lines represent the amplitudes at the rubbery state and glassy state, respectively. The dash lines represent the expected amplitudes in the intermediate states. (For interpretation of the references to colour in this figure legend, the reader is referred to the web version of this article.)

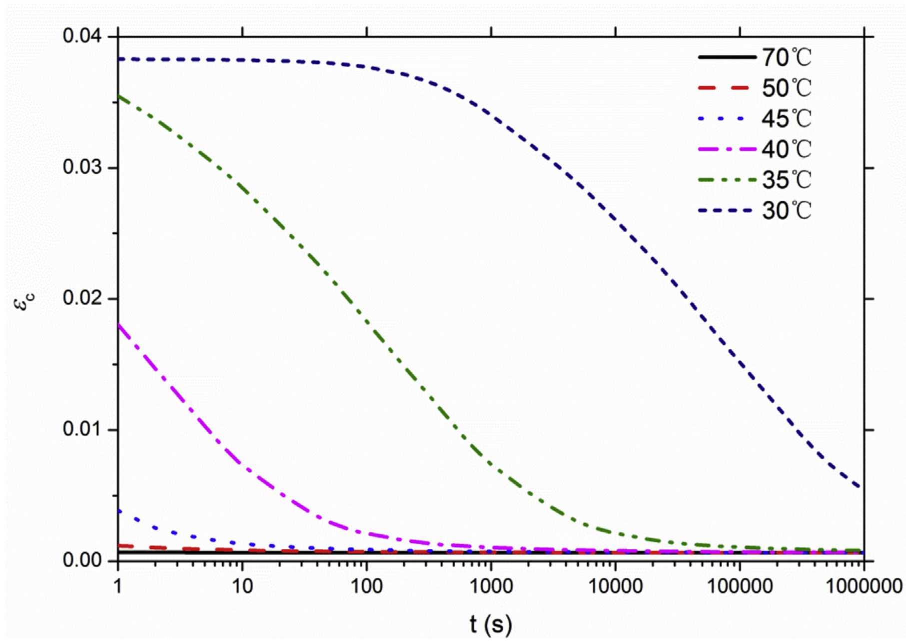

Fig. 10. Critical buckling strains of the thin Si film on the SMP substrate as a function of relaxed time at different temperatures.

the Young's modulus of the SMP substrate is decreasing during the relaxation, while the Young's modulus of the Si film keeps constant. After relaxed for enough time, the SMP substrate will end with the properties of its rubbery state, and the Young's modulus of the substrate as well as the critical buckling strain will not change any more.

3.4. Buckling evolution

From our study, we find that the changing rate of the buckling geometry depends on the temperature of the SMP substrate, which means that the buckling geometry changes faster and reaches equilibrium more quickly at a higher temperature. To prove this, we adopt the assumption that the buckling occurs instantaneously, and perform theoretical analysis as follows. The Young's moduli and Poisson's ratios of SMP substrate at different temperatures are taken as the values after relaxed for a certain time.

Considering a Si film with thickness of 100 nm on the SMP substrate, from the theory analysis in Section 2, we know that the critical buckling strain can be determined by $\varepsilon_c = \frac{1}{4}(3\overline{E}_s/\overline{E}_f)^{\frac{2}{3}}$ with previous theory. Thus, combining with the SMP theory in Section 3.1, the critical strain at glassy state can be calculated as $\varepsilon_{c0} = 0.035988$. Thus, applying a pre-strain of $\varepsilon_{pre} = 0.035988$ to the SMP substrate, the film should buckle at all temperatures (70 °C, 50 °C, 45 °C, 40 °C, 35 °C and 30 °C). However, with the present theory, we can deduce that the true critical buckling strains at glassy state is $\varepsilon_{c0}^{true} = 0.038291$ with Eq. (50). Thus, the pre-strain is smaller than the true critical buckling strain at glassy state, and no buckling should appear. The wavelengths and amplitudes of the buckling geometry after the SMP substrate relaxed for corresponding time can be calculated utilizing Eqs. (52) and (53), and the results are shown as the solid line in Fig. 11.

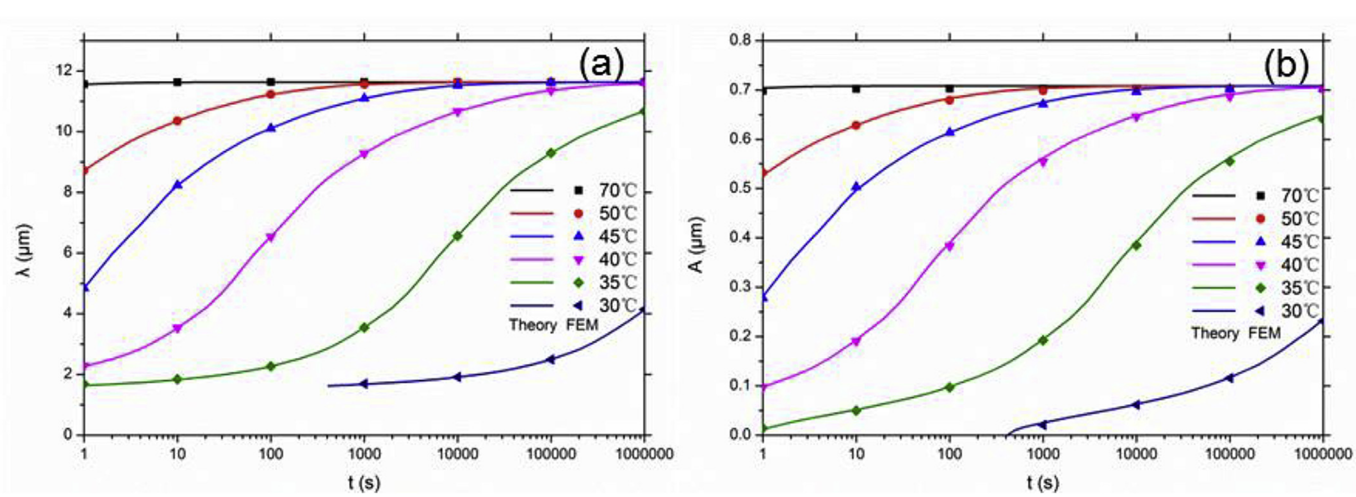

Fig. 11. (a) Wavelength and (b) Amplitude of Si film on SMP substrate as a function of time at different temperatures. The pre-strain is $\varepsilon_{c0} = 0.035988$ and the thickness of Si film is 100 nm. The wavelengths and amplitudes are obtained by employing the Young's moduli and Poisson's ratio at corresponding time. The solid lines represent the theoretical prediction and the dots represent the simulation results.

Furthermore, to prove that the true critical buckling strain ε_c^{true} in present theory is correct, finite element simulations are implemented in the commercial software ABAQUS. In the modeling, the thickness of the SMP substrate and Si film are $h_s = 20$ μm and $h_f = 100$ nm, respectively, which gives $h_s/h_f = 200$ and can be treated as infinitely thick substrate according to Huang (2005). The initial length L_0 of the substrate is approximately 10λ (λ is the calculated wavelength of the buckling geometry) and the length of the Si film is $L=(1+\varepsilon_{pre})L_0$. Considering plane-strain problem in the simulation, the thin Si film and SMP substrate are all modeled as the 8-node plane-strain element (CPE8). The FEM simulation results are presented as the dots in Fig. 11.

From the finite element simulation and theoretical results as shown in Fig. 11, we could find following phenomena. First, with the same pre-strain applied to the substrate, both the wavelength and amplitude of the film on the SMP substrate at 30 °C increase slowly as the relaxation time of the SMP substrate increases, and the buckling geometry could be treated as equilibrium (as stated in Section 3.2, the film buckles immediately at the glassy state and reaches equilibrium) for a short relaxation time; While the wavelength and amplitude of the film on the SMP substrate at a higher temperature change much more quickly and significantly, and the changing of buckling geometry at 70°C could be understood as happening instantaneously. Second, the wavelengths and amplitudes of the film on the SMP substrate at any temperature will finally reach constant values, when the SMP substrate becomes rubbery after relaxed for enough time. Third, the pre-strain is taken as the critical buckling strain calculated with $\varepsilon_c = \frac{1}{4}(3\overline{E}_s/\overline{E}_f)^{\frac{2}{3}}$ at 30 °C ($\varepsilon_{c0} = 0.035988$), which is lower than the true critical buckling strain as predict with the improved theory ($\varepsilon_{c0}^{true} = 0.038291$), thus the buckling doesn't occur at the very first for the film on the SMP substrate at 30 °C (the finite element results also can prove this) but appears after some time instead, because the critical buckling strain will decrease after the SMP substrate relaxed as shown in Fig. 10; This could be understood as that the stress relaxation in the SMP substrate can trigger the buckling of the film on it.

4. Programming of the controlled buckling

From the theoretical analysis in Section 3, we know that the critical buckling strain $\varepsilon_{c0} = 0.038291$ at glassy state is larger than the critical buckling strain $\varepsilon_{c\infty} = 6.722 \times 10^{-4}$ at rubbery state. Thus, if the pre-strain ε_{pre} applied to the SMP substrate is between these two critical buckling strains, the thin film will form buckling at rubbery state (high temperature) and no buckling at glassy state (low temperature). Therefore, when the pre-strain ε_{pre} applied to the SMP substrate is between these two critical buckling strains, we can use the following programming process to control the buckling of the thin film on the SMP substrate.

The programming process is schematically plotted in Fig. 12. First, we put a flat thin film on the pre-stretched substrate and bond them together at a high temperature (70 °C, the substrate is at the rubbery state). Second, the substrate and film is cooled to a low temperature (30 °C, the substrate is at the glassy state). Third, release the pre-strain to let the substrate recover its initial length along with the film. Fourth, reheat the substrate and film to the high temperature.

The steps in the red rectangle (①→②→③), which are the same as those in Fig. 1, represent the general process to form film buckling on a compliant substrate. As long as the pre-strain is larger than $\varepsilon_{c\infty}$, the film on the substrate will form buckles. If the pre-strain is between $\varepsilon_{c\infty}$ and ε_{c0}, after cooling (②→④), the film will have no buckles and remain flat after releasing the pre-strain at the low temperature (④→⑤), because the pre-strain is smaller than

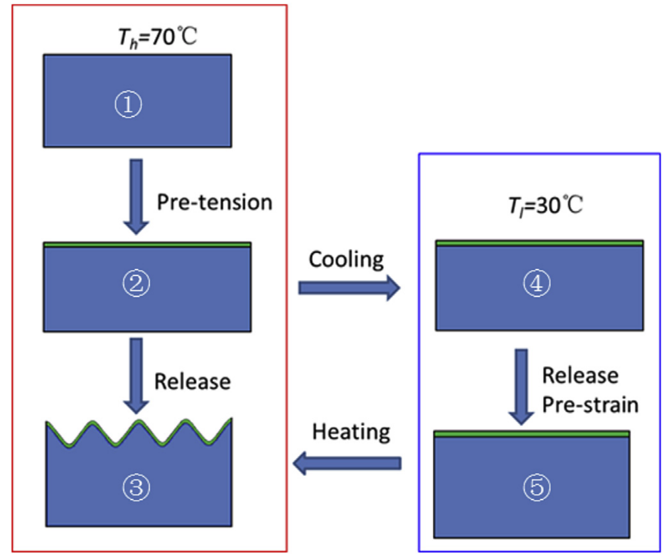

Fig. 12. A schematic of the programming process for the controlled buckling (①→②→③ represent the general process to form film buckling on a compliant substrate and ①→②→④→⑤→③ constitute the programming process to control the buckling of film on SMP substrate).

the critical buckling strain in glassy state. However, if the pre-strain is larger than ε_{c0}, the film will also form buckles upon releasing the pre-strain in glassy state (at low temperature). The flat film in ⑤ can form buckles automatically during the reheating process, and finally grows to be the same as that in the rubbery state ③. Thus, ①→②→④→⑤→③ constitute the complete programming process to control the buckling of film on SMP substrate. From the results in Fig. 9, we can know that the control is effective for a pre-strain between $\varepsilon_{c\infty}$ and ε_{c0}.

The programming process to control the buckling of thin Si film on SMP substrate is realized with finite element methods through the commercial software ABAQUS and the finite element model is the same as in Section 3. Fig. 13 displays the deformation contours at different stages of the programming.

In Fig. 13, (a) displays the deformed geometry after the Si film of initial length bonded to the stretched SMP substrate at 70 °C. (b) represents the geometry of the Si/SMP structure after cooled to 30 °C. (c) shows the geometry of the Si/SMP structure after released the pre-strain. (d)~(h) display the buckling patterns after heating for different periods of time during the recovery process, from which we could see the buckling evolution process with temperature increasing. At first, though the buckling is not stable, we can find that the wavelength of the buckling is small, and this is consistent with the theoretical and finite element results based on assuming the buckling occurs instantaneously. As the temperature increases, the wavelength becomes larger and wave numbers decrease. Finally, the buckling ends up with a stable pattern (in rubbery state) as shown in Fig. 13 (h).

5. Concluding remarks

In this paper, we have introduced the theoretical study and finite element simulations for the buckling of a thin film on the compliant substrate. A continuum mechanics theory for large deformation buckling is established based on minimizing the total energy of the film and substrate, and considering the precise curvature of the buckled film and the Poisson's ratio of the substrate. The prediction results using this proposed theory agree quite well with previous experimental results. Furthermore, the modified

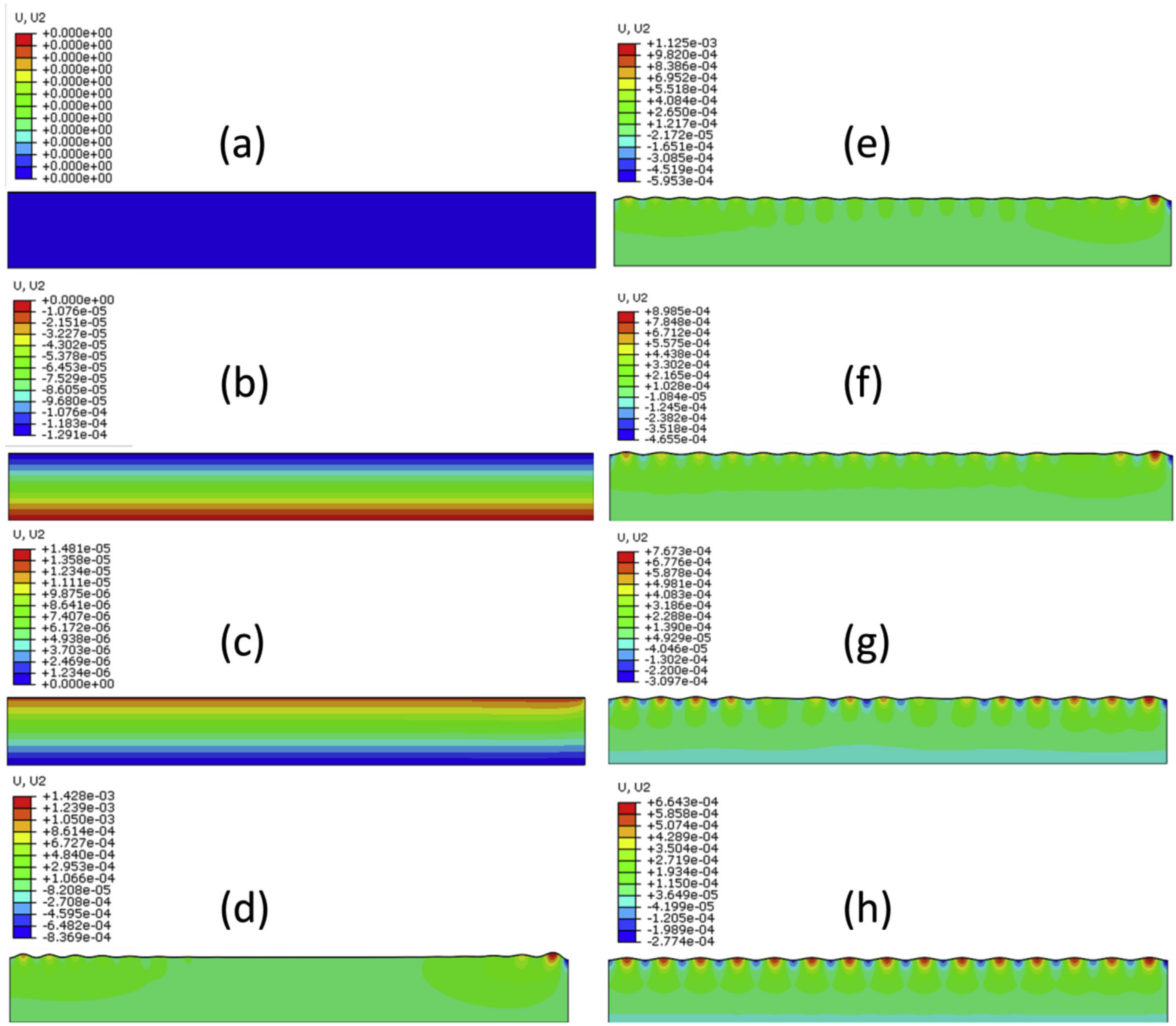

Fig. 13. The deformed shape of the Si/SMP structure at different stages of the programming (the colour indicate the displacement on the vertical direction). (a) The Si film of initial length is bonded to the stretched SMP substrate at 70 °C. (b) The Si/SMP structure is cooled to 30 °C while keeping the length constant. (c) The pre-strain of the SMP substrate is released at 30 °C. (d)~(h) The evolution of buckling during the heating process from 30 °C to 70 °C. (For interpretation of the references to colour in this figure legend, the reader is referred to the web version of this article.)

theory is proposed to simplify the expressions for the wavelength and amplitude of the buckled geometry. Under the assumption of that the buckling occurs instantaneously, we have studied the buckling behavior of thin Si film on SMP substrate both in theoretical analysis and finite element simulations. The mechanism of buckling evolution is investigated and it can give us a better understanding of the buckling process. We also find that the critical buckling strain at glassy state is larger than rubbery state. According to this finding, a programmed method to control the buckling of thin film on the SMP substrate is proposed and realized with finite element simulation. The simulation results also display the evolution process of buckling of thin film on SMP substrate.

Acknowledgements

The authors are grateful for the support from the National Natural Science Foundation of China through grant numbers 11372236, 11572236 and 11321062.

References

Alireza, B., Faramarz, G., 2015. Switching band-gaps of a phononic crystal slab by surface instability. Smart Mater. Struct. 24 (7), 075009.
Bowden, N., Brittain, S., Evans, A.G., Hutchinson, J.W., Whitesides, G.M., 1998. Spontaneous formation of ordered structures in thin films of metals supported on an elastomeric polymer. Nature 393 (6681), 146–149.
Bowden, N., Huck, W.T.S., Paul, K.E., Whitesides, G.M., 1999. The controlled formation of ordered, sinusoidal structures by plasma oxidation of an elastomeric polymer. Appl. Phys. Lett. 75 (17), 2557–2559.
Chatterjee, S., McDonald, C., Niu, J., Velankar, S.S., Wang, P., Huang, R., 2015. Wrinkling and folding of thin films by viscous stress. Soft Matter 11 (9), 1814–1827.
Chen, C., Tao, W., Liu, Z.J., Zhang, Y.W., Song, J., 2011. Controlled buckling of thin film on elastomeric substrate in large deformation. Theor. Appl. Mech. Lett. 1 (2), 021001.

Chen, X., Hutchinson, J.W., 2004. Herringbone buckling patterns of compressed thin films on compliant substrates. J. Appl. Mech. 71 (5), 597–603.
Chen, Y., Liu, Y., Yan, Y., Zhu, Y., Chen, X., 2016. Helical coil buckling mechanism for a stiff nanowire on an elastomeric substrate. J. Mech. Phys. Solids 95, 25–43.
Chen, Y.C., Crosby, A.J., 2014. High aspect ratio wrinkles via substrate prestretch. Adv. Mater 26 (32), 5626–5631.
Chen, Z., Kim, Y.Y., Krishnaswamy, S., 2012. Anisotropic wrinkle formation on shape memory polymer substrates. J. Appl. Phys. 112 (12), 124319.
Cheng, H., Song, J., 2013. A simply analytic study of buckled thin films on compliant substrates. J. Appl. Mech. 81 (2), 024501.
Cheng, H., Zhang, Y., Hwang, K.-C., Rogers, J.A., Huang, Y., 2014. Buckling of a stiff thin film on a pre-strained bi-layer substrate. Int. J. Solids Struct. 51 (18), 3113–3118.
Chiche, A., Stafford, C.M., Cabral, J.T., 2008. Complex micropatterning of periodic structures on elastomeric surfaces. Soft Matter 4 (12), 2360–2364.
Chua, D.B.H., Ng, H.T., Li, S.F.Y., 2000. Spontaneous formation of complex and ordered structures on oxygen-plasma-treated elastomeric polydimethylsiloxane. Appl. Phys. Lett. 76 (6), 721–723.
Diani, J., Gilormini, P., Frédy, C., Rousseau, I., 2012. Predicting thermal shape memory of crosslinked polymer networks from linear viscoelasticity. Int. J. Solids Struct. 49 (5), 793–799.
Dickson, M., 2015. Compressive buckling converts 2d microstructures and nanostructures into 3d. MRS Bull. 40 (03), 203.
Fu, C.C., Anthony, G., Long, M., Ferri, C.G.L., Rich, B.D., Somnath, G., Sayantani, G., Lee, L.P., Ajay, G., Michelle, K., 2009. Tunable nanowrinkles on shape memory polymer sheets. Adv. Mater 21 (21), 4472–4476.
Groenewold, J., 2001. Wrinkling of plates coupled with soft elastic media. Phys. A 298 (1), 32–45.
Harrison, C., Stafford, C.M., Zhang, W., Karim, A., 2004. Sinusoidal phase grating created by a tunably buckled surface. Appl. Phys. Lett. 85 (18), 4016–4018.
He, Y.H., Guo, S.S., Liu, Z.S., Liew, K.M., 2015. Pattern transformation of thermo-responsive shape memory polymer periodic cellular structures. Int. J. Solids Struct. 71, 194–205.
Huang, R., 2005. Kinetic wrinkling of an elastic film on a viscoelastic substrate. J. Mech. Phys. Solids 53 (1), 63–89.
Huang, R., Im, S.H., 2006. Dynamics of wrinkle growth and coarsening in stressed thin films. Phys. Rev. E 74 (2), 026214.
Huang, R., Suo, Z., 2002a. Instability of a compressed elastic film on a viscous layer. Int. J. Solids Struct. 39 (7), 1791–1802.
Huang, R., Suo, Z., 2002b. Wrinkling of a compressed elastic film on a viscous layer. J. Appl. Phys. 91 (3), 1135–1142.
Huang, X., Li, B., Hong, W., Cao, Y.-P., Feng, X.-Q., 2016. Effects of tension–compression asymmetry on the surface wrinkling of film–substrate systems. J. Mech. Phys. Solids 94, 88–104.
Huang, Z.Y., Hong, W., Suo, Z., 2004. Evolution of wrinkles in hard films on soft substrates. Phys. Rev. E 70 (3), 030601.
Huang, Z.Y., Hong, W., Suo, Z., 2005. Nonlinear analyses of wrinkles in a film bonded to a compliant substrate. J. Mech. Phys. Solids 53 (9), 2101–2118.
Im, S.H., Huang, R., 2005. Evolution of wrinkles in elastic-viscoelastic bilayer thin films. J. Appl. Mech. 72 (6), 955–961.
Jiang, H., Khang, D.-Y., Fei, H., Kim, H., Huang, Y., Xiao, J., Rogers, J.A., 2008a. Finite width effect of thin-films buckling on compliant substrate: experimental and theoretical studies. J. Mech. Phys. Solids 56 (8), 2585–2598.
Jiang, H., Khang, D.-Y., Song, J., Sun, Y., Huang, Y., Rogers, J.A., 2007a. Finite deformation mechanics in buckled thin films on compliant supports. PNAS 104 (40), 15607–15612.
Jiang, H., Sun, Y., Rogers, J.A., Huang, Y., 2007b. Mechanics of precisely controlled thin film buckling on elastomeric substrate. Appl. Phys. Lett. 90 (13), 133119.
Jiang, H., Sun, Y., Rogers, J.A., Huang, Y., 2008b. Post-buckling analysis for the precisely controlled buckling of thin film encapsulated by elastomeric substrates. Int. J. Solids Struct. 45 (7–8), 2014–2023.
Jiang, W., Li, Z., 2009. A numerical study of the wrinkling evolution of an elastic film on a viscous layer. Modell. Simul. Mater. Sci. Eng. 17 (5), 055010.
Khang, D.Y., Rogers, J.A., 2006. A stretchable form of single-crystal silicon for high-performance electronics on rubber substrates. Science 311 (5758), 208–212.
Kim, K.-S., Lin, Z., Shrotriya, P., Sundararajan, S., Zou, Q., 2008. Iterative control approach to high-speed force-distance curve measurement using afm: time-dependent response of pdms example. Ultramicroscopy 108 (9), 911–920.
Li, J., An, Y., Huang, R., Jiang, H., Xie, T., 2012. Unique aspects of a shape memory polymer as the substrate for surface wrinkling. ACS Appl. Mater. Interfaces 4 (2), 598–603.
Liu, Z.S., Hong, W., Suo, Z., Swaddiwudhipong, S., Zhang, Y.W., 2010. Modeling and simulation of buckling of polymeric membrane thin film gel. Comput. Mater. Sci. 49 (1), S60–S64.
Liu, Z.S., Swaddiwudhipong, S., Cui, F.S., Hong, W., Suo, Z., Zhang, Y.W., 2011. Analytical solutions of polymeric gel structures under buckling and wrinkle. Int. J. Appl. Mech. 3 (02), 235–257.
Liu, Z.S., Swaddiwudhipong, S., Hong, W., 2013. Pattern formation in plants via instability theory of hydrogels. Soft Matter 9 (2), 577–587.
Liu, Z.S., Toh, W., Ng, T.Y., 2015. Advances in mechanics of soft materials: a review of large deformation behavior of hydrogels. Int. J. Appl. Mech. 7 (05), 1530001.
Low, S.-H., Lau, G.-K., 2014. Bi-axially crumpled silver thin-film electrodes for dielectric elastomer actuators. Smart Mater. Struct. 23 (12), 125021.
Mokni, N., Kostrzewa, M., Sidoroff, F., 2008. Instability of an elastic film on a viscous layer. Eur. J. Mech. A. Solids 27 (5), 783–795.
Ou, Z., Yao, X., Zhang, X., Fan, X., 2016. Dynamic stability of flexible electronic structures under step loads. Eur. J. Mech. A. Solids 58, 247–255.
Park, H.-J., Son, C., Ha, M.-Y., Park, S.-H., 2015. Effective formation of hierarchical wavy shapes using weak photopolymerization and gradual thermal curing process. Mater. Lett. 141, 47–54.
Song, J., Jiang, H., Huang, Y., Rogers, J.A., 2009. Mechanics of stretchable inorganic electronic materials. J. Vac. Sci. Technol. A 27 (5), 1107–1125.
Song, J., Jiang, H., Liu, Z.J., Khang, D.Y., Huang, Y., Rogers, J.A., Lu, C., Koh, C.G., 2008. Buckling of a stiff thin film on a compliant substrate in large deformation. Int. J. Solids Struct. 45 (10), 3107–3121.
Stafford, C.M., Harrison, C., Beers, K.L., Karim, A., Amis, E.J., VanLandingham, M.R., Kim, H.-C., Volksen, W., Miller, R.D., Simonyi, E.E., 2004. A buckling-based metrology for measuring the elastic moduli of polymeric thin films. Nat. Mater. 3 (8), 545–550.
Stafford, C.M., Vogt, B.D., Harrison, C., Huang, R., 2006. Elastic moduli of ultrathin amorphous polymer films. Macromolecules 39 (15), 5095–5099.
Sun, Y., Choi, W.M., Jiang, H., Huang, Y.Y., Rogers, J.A., 2006. Controlled buckling of semiconductor nanoribbons for stretchable electronics. Nat. Nanotechnol. 1 (3), 201–207.
Timoshenko, S.P., 1961. Theory of Elastic Stability. McGraw-Hill, New York.
Wang, J.-W., Li, B., Cao, Y.-P., Feng, X.-Q., 2015a. Surface wrinkling patterns of film–substrate systems with a structured interface. J. Appl. Mech. 82 (5), 051009.
Wang, Q., Zhao, X., 2016. Beyond wrinkles: multimodal surface instabilities for multifunctional patterning. MRS Bull. 41 (02), 115–122.
Wang, S., Huang, Y., Rogers, J.A., 2015b. Mechanical designs for inorganic stretchable circuits in soft electronics. IEEE Trans. Compon. Packag. Manuf. Technol. 5 (9), 1201–1218.
Wang, Y., Feng, X., 2009. Dynamic behaviors of controllably buckled thin films. Appl. Phys. Lett. 95 (23), 231915.
Wilder, E.A., Guo, S., Lin-Gibson, S., Fasolka, M.J., Stafford, C.M., 2006. Measuring the modulus of soft polymer networks via a buckling-based metrology. Macromolecules 39 (12), 4138–4143.
Xie, T., Xiao, X., Li, J., Wang, R., 2010. Encoding localized strain history through wrinkle based structural colors. Adv. Mater 22 (39), 4390–4394.
Xu, S., Yan, Z., Jang, K.-I., Huang, W., Fu, H., Kim, J., Wei, Z., Flavin, M., McCracken, J., Wang, R., 2015. Assembly of micro/nanomaterials into complex, three-dimensional architectures by compressive buckling. Science 347 (6218), 154–159.
Yang, D., He, L.H., 2014. Photo-triggered wrinkling of glassy nematic films. Smart Mater. Struct. 23 (4), 045012.
Yoo, P.J., Suh, K.Y., Park, S.Y., Lee, H.H., 2002. Physical self-assembly of microstructures by anisotropic buckling. Adv. Mater 14 (19), 1383–1387.
Zhang, N.-H., Chen, J.-Z., 2009. Elastic bending analysis of bilayered beams by an alternative two-variable method. Eur. J. Mech. A. Solids 28 (2), 284–288.
Zhao, Y., Huang, W.M., Fu, Y.Q., 2011. Formation of micro/nano-scale wrinkling patterns atop shape memory polymers. J. Micromech. Microeng. 21 (6), 67007–67014.
Zhou, Y.-N., Huang, G.-Y., 2014. Buckling of elastic thin films on compliant substrates for determination of surface parameters. Chin. Phys. Lett. 31 (11), 116202.